Journal of the Optical Society of Korea, Vol. 10, No. 1, March 2006, pp. 16-22

# Investigation of Performance Degradation of Shack Hartmann Wavefront Sensing Due to Pupil Irradiance Profile

Jun Ho Lee*

*Dept. of Applied Optical Science, Kongju National University, Kongju-si, Chungnam, South KOREA*

Young Cheol Lee and Eung Cheol Kang

*Agency for Defense Development, P.O. Box 356, Yuseong, Daejeon, South KOREA*

(Received December 2, 2005 : revised January 5, 2006)

Wavefront sensing using a Shack-Hartmann sensor has been widely used for estimating wavefront errors or distortions. The sensor combines the local slopes, which are estimated from the centroids of each lenslet image, to give the overall wavefront reconstruction. It was previously shown that the pupil-plane irradiance profile effects the centroid estimation. Furthermore, a previous study reported that the reconstructed wavefront from a planar wavefront with a Gaussian pupil irradiance profile contains large focus and spherical aberration terms when there is a focus error. However, it has not been reported yet how seriously the pupil irradiance profiles, which can occur in practical applications, effect the sensing errors. This paper considered two cases when the irradiance profiles are not uniform: 1) when the light source is Gaussian and 2) when there is a partial interference due to a double reflection by a beam splitting element. The images formed by a Shack-Hartmann sensor were simulated through fast Fourier transform and were then supposed to be detected by a noiseless CCD camera. The simulations found that sensing errors, due to the Gaussian irradiance profile and the partial interference, were found to be smaller than RMS $\lambda/50$ when $\lambda$ is 0.6328 μm, which can be ignored in most practical cases where the reference and test beams have the same irradiance profiles.

*OCIS codes* : 010.1080, 070.2580, 120.5050, 220.4840

## I. INTRODUCTION

Shack-Hartmann sensors have been extensively used in a very wide range of applications including adaptive optics [1], lens testing [2] and ocular aberrometry [3]. They measure wavefront aberrations by use of an array of subapertures (lenslets). The lenslets focus light onto a detector array, where the centroid of the spot formed behind each lenslet is used as a measure of the phase mean gradient in the subaperture. Different sources including read-out noise, the finite CCD and window size, misalignments and low-photon flux cause errors in estimating the centroid and some studies were devoted to decreasing the errors [4-10].

For adaptive optics applied to compensate atmospheric distortions, the incoming wavefront can be assumed to have uniform intensity over the entrance pupil without loss of measurement accuracy. However, there are some applications, such as Gaussian beam, where the pupil irradiance profiles cannot be considered to be uniform anymore. A previous study reported that the reconstructed wavefront from a planar wavefront with a Gaussian pupil irradiance profile contains large focus and spherical aberration terms. However, the aberrations were shown to arise only when there is a focus error [11], which is contrary to our herein result that a planar wavefront with a Gaussian pupil irradiance causes in aberrations in reconstructed wavefront even when there is no focus error.

In this paper, we simulated the effects of the variance of pupil irradiance profile due to the characteristics of laser sources and partial interferences, which are sometimes hard to remove in practical applications.

## II. THEORETICAL DESCRIPTIONS AND ITS SIMULATION

### 1. Theoretical descriptions

The centroid implies the measure of the first moment

of the focal-plane irradiance pattern ($I_j(u, \nu)$) for each subaperture, as shown in Fig. 1. Accordingly, the centroid in the $u$-direction $j$ in the th subaperture, designated $C_u^j$, is calculated as:

$$C_u^j = \frac{\iint u I_j(u,\nu) du d\nu}{\iint I_j(u,\nu) du d\nu} \tag{1}$$

where the integration is over the entire region of the focal plane associated with the jth subaperture. Eq. (1) holds equally for the ν component centroid, substituting $u$ for ν in the integral.

The centroid is related with the irradiance distribution ($I_j(x, y)$) and the spatial phase ($\phi_j(x, y)$) of the impinging field as follows [12].

$$C_u^j = \frac{\iint W_j(x,y)\, I_j(x,y) \nabla_x \phi_j(x,y) dx dy}{\iint W_j(x,y)\, I_j(x,y) dx dy} \tag{2}$$

where λ is the wavelength of the light, $f$ is the focal length of the lens, $\nabla_x \phi_j(x, y)$ is the x-derivative of the phase in the $f$ th subaperture, $W_j(x, y)$ is the pupil weighting function associated with the jth subaperture, which is 1 inside the subaperture and 0 otherwise.

Eq. (2) can be simplified only when the pupil-plane irradiance is uniform over the extent of the subaperture as follows.

$$C_w^j = \frac{\lambda f}{2\pi} \frac{\iint W_j(x,y) I_j(x,y) \nabla_x \phi_j(x,y) dx dy}{\iint W_j(x,y) I_j(x,y) dx dy} \tag{3}$$

where $A_s$ is the area of the subaperture area and $\frac{\iint W_j(x,y) \nabla_x \phi_j(x,y) dx dy}{A_s}$ is the mean average of x-derivative of the phase in the $j$ th subaperture.

Therefore the centroid is directly proportional to the mean derivative of the phase only when the pupil-plane irradiance is uniform. Otherwise the centroid represents the weighted average of the phase gradient over the subaperture.

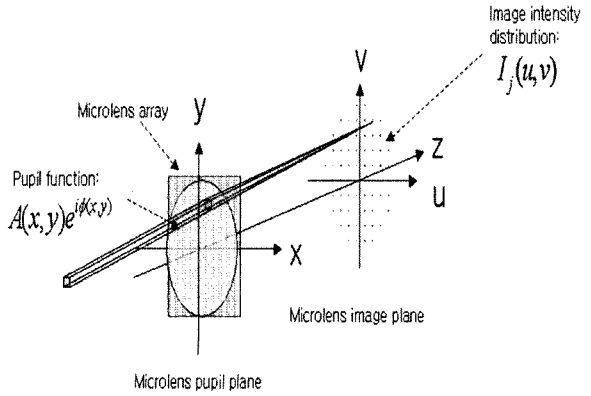


FIG. 1. Schematic of the relationship between the pupil plane and the image plane.

## 2. Computer simulation of image forming by an array of microlens

The simulation arrangement consists of a circular collimated optical field (λ=0.6328 μm) of 4.5 mm diameter impinging on an array of square microlenses with focal length of 7.6 cm and side length of 300 μm [13]. The CCD detector plane was placed at the focal plane of the lens.

We first generate a circular entrance pupil function $A(x, y)e^{i\phi(x,y)}$, where $A(x, y)$ is the amplitude function and $\phi(x, y)$ is the phase function, into a 7680×7680 sampled rectangular matrix. Then each subaperture pupil function $A_j(x, y)e^{i\phi(x,y)}$ was re-sampled into a 256×256 rectangular matrix, which was centered into a zero-padded 1024×1024 rectangular matrix, and the image of each subaperture or Point Spread Function (PSF) was computed through the Fast Fourier transform of the subaperture pupil function. The image was then supposed to be detected by a noiseless CCD camera with 10 μm pixel size. The all sub-aperture images were then merged to give the CCD image by the array of microlenses. The intensity maximum of the final image was set to 256 to simulate an optimal use of the detection dynamic range of the camera. Fig. 2 shows 6 major steps in the simulation. The similar simulation method was used in simulating a pyramidal wavefront sensor [15].

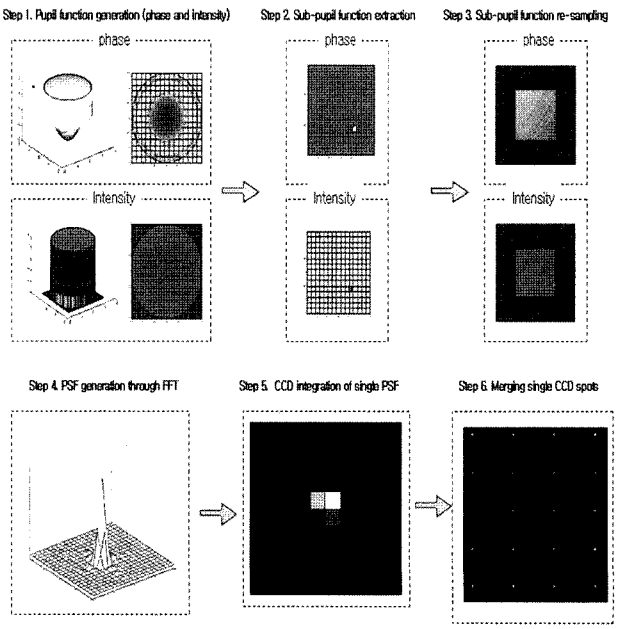


FIG. 2. The simulation steps of image forming by an array of microlenses.

### 3. Computer simulation of image reconstruction

A pupil phase function $\phi$ can be represented by its approximate conjugate $\hat{\phi}$ that is the summation of Zernike polynomials $Zi$ (following Noll's definition [14]) as

$$\hat{\phi} = \sum_i a_i Zi \tag{4}$$

In this computer simulation, the Zernike coefficients $a_i$ were reconstructed from minimizing the RMS (root mean square) centroids errors as given by Eq. (5) and 30 Zernike polynomials were used in the calculation.

$$e^2 = \int \rho d\rho \int d\theta W(\rho)\left(\left[\triangle C_u^j(\phi) - \triangle C_u^j(\hat{\phi})\right]^2 + \left[\triangle C_\nu^j(\phi) - \triangle C_\nu^j(\hat{\phi})\right]^2\right) \tag{5}$$

$$\triangle C_u^j = \lfloor C_u^j \rfloor_{test} - \lfloor C_u^j \rfloor_{reference} \tag{6}$$

where $\lfloor C_u^j \rfloor_{test}$ and $\lfloor C_u^j \rfloor_{reference}$ are the centroids of the j-th subaperture of the test and the reference beams in u-direction, respectively. Eq. (6) holds equally for the $\nu$ component centroid, substitution $u$ for $\nu$.

Since the test beam and reference beam might have different irradiance due to the different light sources or the different optical paths, the following simulations were performed for two different cases: 1) when the reference beam is a planar wavefront with an uniform intensity profile and 2) when the reference beam is a planar wavefront with intensity profiles identical to the those of the test beam.

## III. THE EFFECT OF GAUSSIAN PUPIL IRRADIANCE PROFILE IN WAVEFRONT SENSING

A wavefront with a Gaussian irradiance profile has the entrance pupil function $A(x,y)e^{i\phi(x,y)}$ given as follows

$$A(x,y)e^{i\phi(x,y)} = A_0 e^{-(x^2+y^2)/2w^2} e^{i\phi(x,y)} \tag{7}$$

where $A_0$ is the peak intensity and $w$ is the relative beam radius at $A(x,y) = A_0/e$ referred to the pupil radius, which is called as 'relative Gaussian beam width'. Fig. 3 (a) shows the relative intensity at the edge of the pupil to the peak intensity as the relative Gaussian beam width $w$ varies. Fig. 3 (b) shows the relative intensity variation across the pupil when the relative beam width $w$ is 1.2. In this case there is 50% relative intensity difference at the edge.

### 1. When the reference beam is a planar wavefront with a uniform intensity profile

The reference beam here was assumed to be ideal i.e., a planar wavefront with a uniform intensity profile. The test beams had Gaussian irradiance profile with seven phase fields: plane ($Z_1$), tilt ($Z_2$), defocus ($Z_4$), coma ($Z_5$), astigmatism ($Z_7$), trefoil ($Z_9$) and spherical aberration ($Z_{11}$). The seven phase fields are of Zernike polynomials and each magnitude of the field is the coefficient of the corresponding Zernike polynomial. The relative Gaussian beam width varied from 0.6 to 4.0 with a step of 0.2. Fig. 4 shows the centroid movements and its reconstructed phase when the relative Gaussian width is 4. From this figure, it is quite clear that even a planar wavefront with a Gaussian irradiance profile can cause focus errors in wavefront sensing.

The sensing errors or phase differences ($e = \phi - \hat{\phi}$) were decomposed by Zernike polynomials as shown in Fig. 5. The sensing errors were found to be independent of phase fields. However, the sensing errors were mainly defocus errors, whose amplitude decreased as the relative Gaussian beam width increased. Fig. 6 shows the RMS

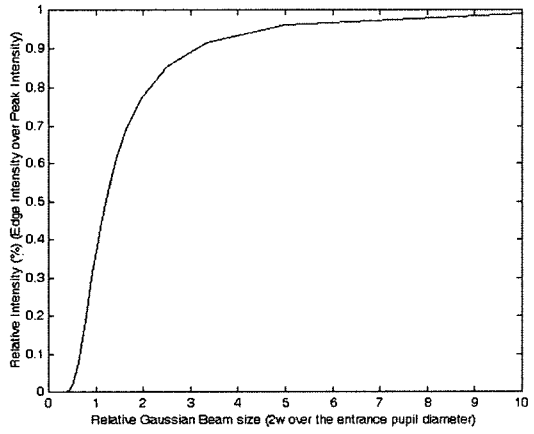


(a) Relative intensity at the edge while the relative beam width $w$ changes.

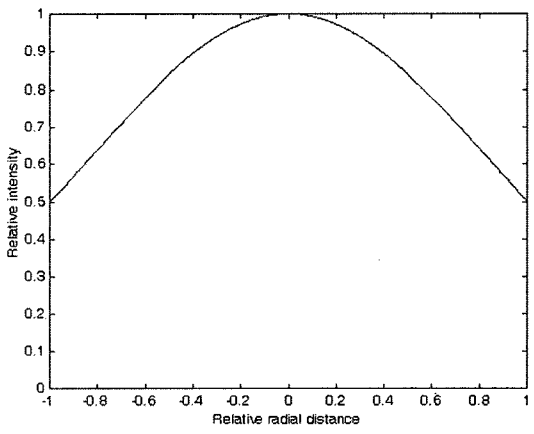


(b) Relative intensity across the pupil when the relative beam width $w$ =1.2.

FIG. 3. The relative intensity variation.

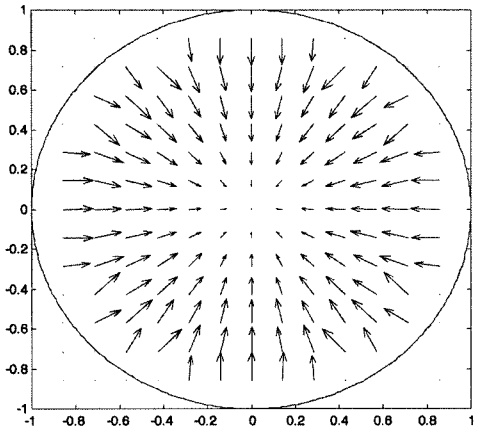

(a) The centroid movements.

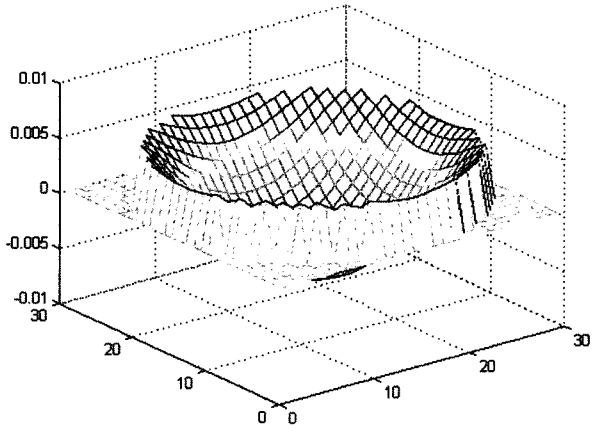

(b) 3D phase field.

FIG. 4. The centroid movements and its reconstructed phase field for a plane wavefront of Gaussian pupil irradiance profile with the relative Gaussian beam width=4.

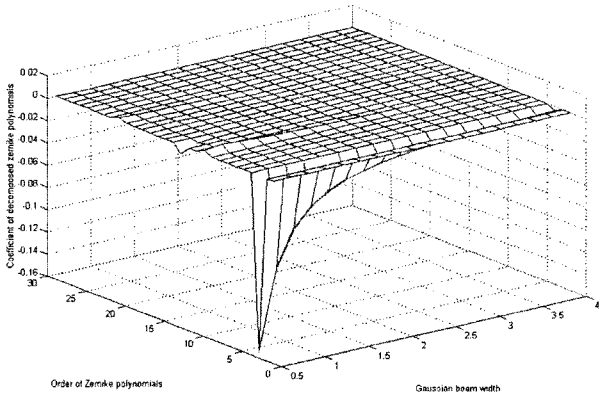


(a) Decomposed Zernike coefficient of the sensing errors.

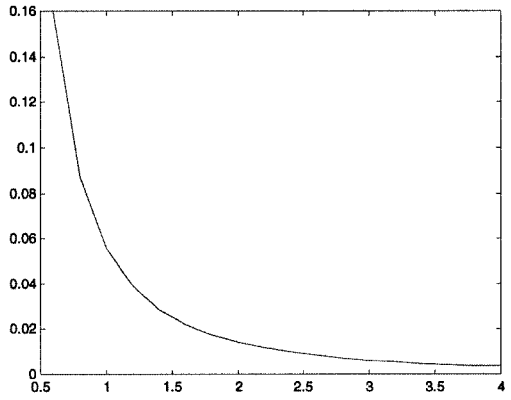

(b) Amplitude of defocus errors in the sensing errors.

FIG. 5. The decomposed Zernike coefficients of the sensing errors or phase difference $s(e = \phi - \hat{\phi})$ when the relative Gaussian beam varied from 0.6 to 4.0 and the coefficients of its major component focus error.

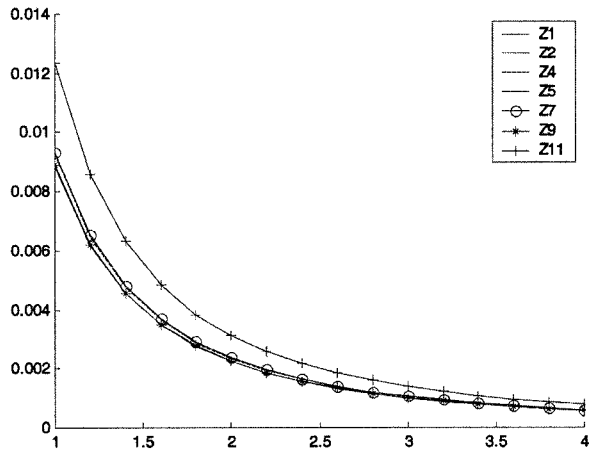


FIG. 6. The RMS wavefront sensing errors in unit of wavelengths for the incoming wavefront with a Gaussian irradiance profile and seven different phase functions; plane ($Z_1$), tilt ($Z_2$), defocus ($Z_4$), coma ($Z_5$), astigmatism ($Z_7$), trefoil ($Z_9$) and spherical aberration ($Z_{11}$).

(root mean squared) sensing errors in unit of wavelengths for the seven phase entrance functions, which can be equated by a best-fit exponential function as follows:

$$RMS \approx 10^{-2w\widehat{0.35}} \text{ when } w > 1 \tag{8}$$

From Eq. (8), the sensing error due to the Gaussian intensity profile is found to be smaller than $\lambda/100$ RMS for low order phase distortions, which can be ignored in most practical applications.

## 2. When the reference beam is a planar wavefront with an intensity profile identical to that of the test beam

Here the reference beam was considered to have the same irradiance profile with the test beam. Fig. 7 shows the decomposed sensing errors for the defocus phase field. The sensing errors for the other phase fields were

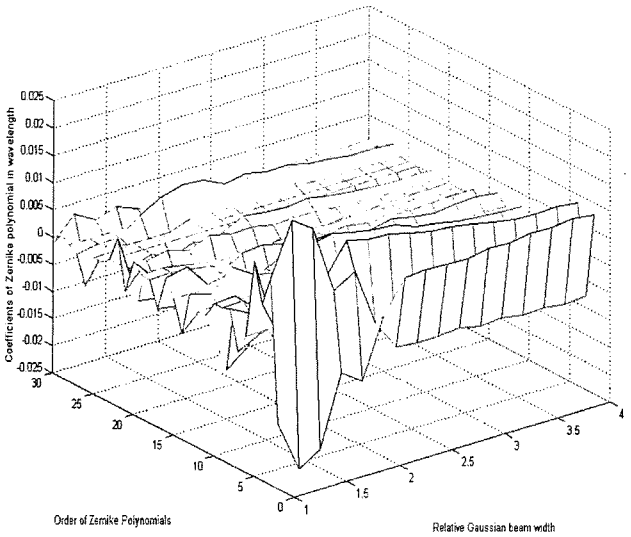


FIG. 7. The decomposed Zernike coefficients of the sensing errors or phase difference s($e = \phi - \hat{\phi}$) when the relative Gaussian beam width varied from 0.6 to 4.0. The reference and test beam had identical Gaussian irradiance profiles.

almost the same. The RMS sensing errors were all smaller than $\lambda/1000$ RMS when the relative Gaussian beam width $w > 1$.

## IV. THE EFFECT OF PARTIAL INTERFERENCES IN WAVEFRONT SENSING

Shack Hartmann sensors have more than one beam splitting element. The beam splitting elements can cause double reflection resulting in the interference in the entrance pupil function and the CCD plane. In most cases, the double-reflected beam has weaker intensity but has tilted phase. Here we use the contrast as defined as follows to quantify the amount of partial interference.

$$C = \frac{I_{\max} - I_{\min}}{I_{\max} + I_{\min}} \tag{9}$$

where $I_{\max}$ and $I_{\min}$ are the maximum and minimum intensity of partially interfered pupil function.

### 1. When the reference beam is a planar wavefront with a uniform intensity profile

The reference beam here was assumed to be ideal i.e., a planar wavefront with a uniform intensity profile. The test beams had uniform irradiance profile with seven phase fields: plane ($Z_1$), tilt ($Z_2$), defocus ($Z_4$), coma ($Z_5$), astigmatism ($Z_7$), trefoil ($Z_9$) and spherical aberration ($Z_{11}$), and the test beams were assumed to be interfered with by their own double-reflected beams. Tilting the original pupil profiles by the amount of $4Z_2$, which causes about 2 fringes, generated by the double-reflected beams. The relative amplitude of the double-reflected beam was changed from 0.2 to 1.0 to change the contrast of the interference.

Fig. 8 shows the fringe pattern and intensity variation at the entrance pupil plane of the Shack-Hartmann sensor when the contrast is 1. Fig. 9 shows the sensing errors or phase difference ($e = \phi - \hat{\phi}$) in terms of Zernike polynomial decomposition as the contrast varied. (The sensing errors were found to be independent ofn the phase fields.). Therefore, when there is a tilted interference in the Shack-Hartmann pupil plane, the information on the tilts should be considered to have errors due to the interferences.

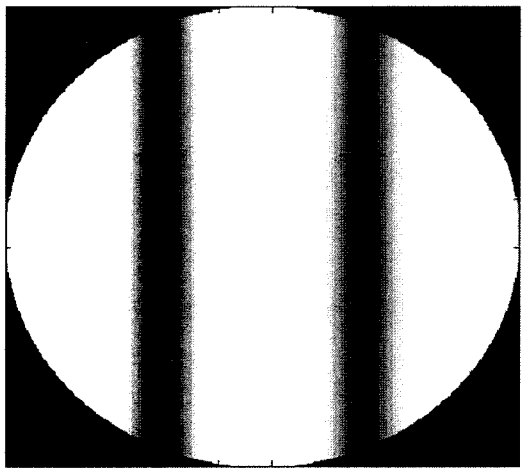

(a) Fringe pattern.

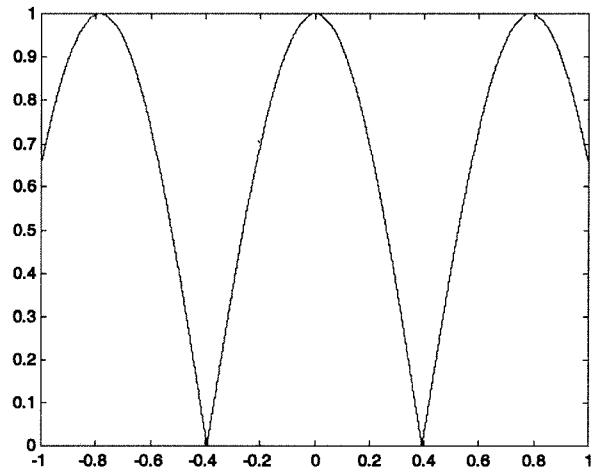


(b) Intensity variation across the pupil.

FIG. 8. Exampled fringe pattern and intensity variation at the entrance pupil plane of the Shack-Hartmann sensor when the beam was interfered with a double-reflected beam. (Contrast=1.0, Tilt=$2Z_2$)

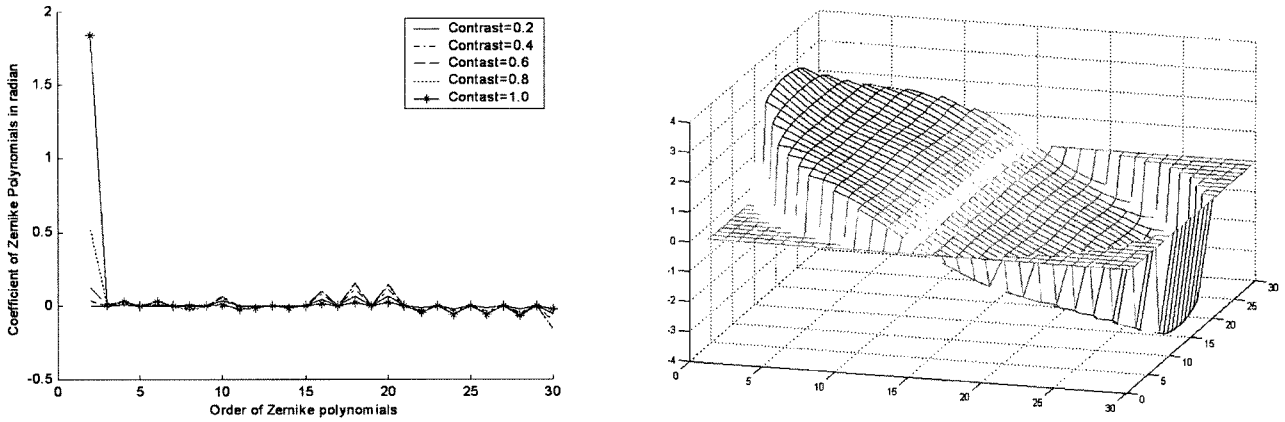


(a) Decomposed sensing errors. (b) Reconstructed wavefront when the contrast is 1.

FIG. 9. Centroid movements and reconstructed wavefront when a planar wavefront was interfered with a double-reflected beam. (Contrast=1.0, Tilt=$2Z_2$)

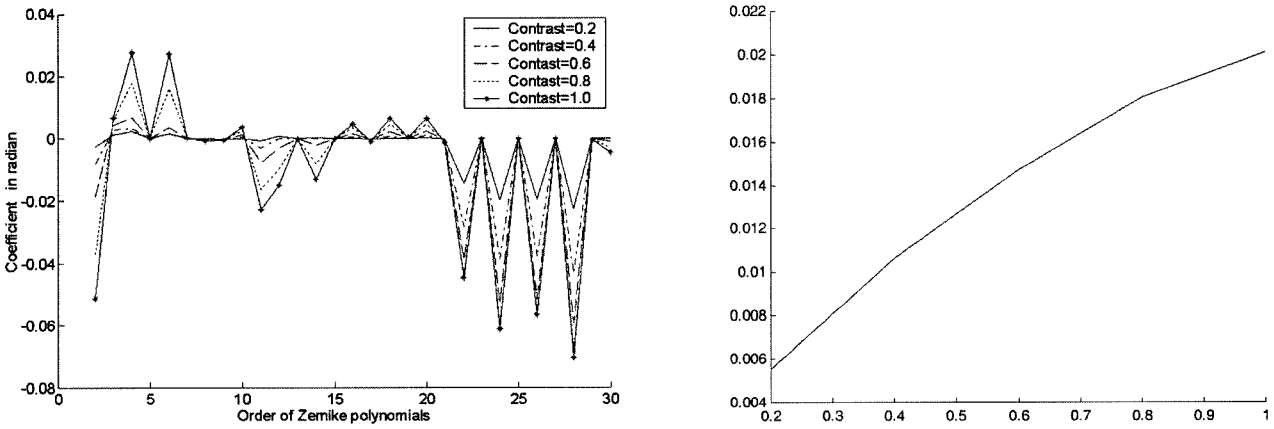


(a) Zernike polynomials. (b) RMS wavefront errors.

FIG. 10. Zernike polynomials of sensing errors or phase difference ($e = \phi - \hat{\phi}$) and RMS wavefront errors as the contrast changed from 0.2 to 1.0.

### 2. When the reference beam is a planar wavefront with an intensity profile identical to that of the test beam

Here the reference beam was considered to have the same irradiance profile with the test beam. Fig. 10 (a) shows the decomposed sensing errors for the defocus phase field. The sensing errors for the other phase fields were almost the same. Fig. 10 (b) shows the RMS sensing errors as the contract changes from 0.2 to 1.0. The RMS sensing errors for all phase fields were found to be smaller than $\lambda/50$ RMS.

## V. CONCLUSION

When the Shack-Hartmann wavefront sensing is performed, the optical layout is usually designed to provide the uniform irradiance profiles at the entrance pupil of the Shack-Hartmann sensor. However, there are some cases when the non-uniformity in the irradiance is inevitable. The most frequent cases are due to Gaussian irradiance profile of a laser and due to the partial interference formed by a double-reflection by beam splitting elements.

This paper found that the sensing errors for low-order phase fields are smaller than $\lambda/50$ RMS in the most practical cases where the test and the reference beams have identical irradiance profiles.

Further researches should follow to investigate the sensing errors under some special conditions such as when there is a significant difference in the beam intensity profiles between the reference and test beams or when the intensity of the sensing noise cannot be ignored compared to that of the beams.

*Corresponding author : jhlsat@kongju.ac.kr

## REFERENCES


[1] J. M. Beckers, "Adaptive Optics for Astronomy: Principles, Performance and Applications," *Annual Review of Astronomy and Astrophysics*, vol. 31, pp. 13-22, 1993.

[2] H. Canabal, J. Alonso, and E. Bernabeu, "Laser beam deflectometry based on a subpixel resolution algorithm," *Opt. Eng.*, vol. 40, pp. 2517-2523, 2001.

[3] E. Moreno-Barriuso and R. Navarro, "Laser ray tracing versus Hartmann-Shack sensor for measuring optical aberrations in the human eye," *J. Opt. Soc. Am.*, vol. 17, pp. 974-985, 2000.

[4] J. S. Morgan, D. C. Slater, J. G. Timothy, and E. B. Jenkins, "Centroid position measurements and subpixel sensitivity variations with the MAMA detector," *Appl. Opt.*, vol. 28, pp.1178-1192, 1989.

[5] G. Cao and X. Yin, "Accuracy analysis of a Hartmann-Shack wavefront sensor operated with a faint object," *Opt. Eng.*, vol. 33, pp. 2331-2335, 1994.

[6] F. Roddier, *Adaptive Optics in Astronomy*, (Cambridge University Press, Cambridge, 1999).

[7] R. Irwan and R. G. Lane, "Analysis of optimal centroid estimation applied Shack-Hartmann sensing," *Appl. Opt.*, vol. 38, pp. 6737-6743, 1999.

[8] J. Arines and J. Ares, "Significance of thresholding process in centroid based gradient wavefront sensors: effective modulation of the wavefront derivative," *Opt. Commun.*, vol. 237, pp. 257-266, 2004.

[9] W.-Y. V. Leung, M. Tallon, and R.G. Lane, "Centroid estimation by model-fitting from undersampled wavefront sensing images," *Opt. Commun.*, vol. 201, pp. 11-20, 2002.

[10] J. Primot, "Theoretical description of Shack-Hartmann wavefront sensor," *Opt. Commun.*, vol. 222, pp. 81-92, 2003.

[11] M. R. Whiteley, "Apparent wavefront aberration of a Gaussian source in a Hartmann wavefront sensor with focus error," *Proc. SPIE*, vol. 4007, pp. 470-480, 2000.

[12] V. I. Tatarskii, "The Effects of the Turbulent Atmosphere on Wave Propagation," (U.S. Department of Commerce, Springfield, 1971).

[13] Adaptive Optics Associates (Ltd).

[14] R. J. Noll, "Zernike polynomials and atmospheric turbulence," *J. Opt. Soc. Am.*, vol. 66, p. 207, 1976.

[15] J. H. Lee, D. D. Walker, and A. P. Doel, "Pupil plane wavefront sensing with a static pyramidal prism : Simulation and preliminary evaluation," *J. Opt. Soc. Korea*, vol. 4, no. 1, pp. 1-6, 2000.